On the Role of Clouds and Moisture in Tropical Waves: A Two-Dimensional Model Study

DANČE ZUROVAC-JEVTIĆ

Program in Atmospheres, Oceans, and Climate, Massachusetts Institute of Technology, Cambridge, Massachusetts, and Department of Meteorology, Stockholm University, Stockholm, Sweden

SANDRINE BONY

Laboratoire de Météorologie Dynamique, Institute Pierre-Simon Laplace, CNRS, Paris, France

KERRY EMANUEL

Program in Atmospheres, Oceans, and Climate, Massachusetts Institute of Technology, Cambridge, Massachusetts

(Manuscript received 2 December 2004, in final form 13 December 2005)

ABSTRACT

Observations show that convective perturbations of the tropical atmosphere are associated with substantial variations of clouds and water vapor. Recent studies suggest that these variations may play an active role in the large-scale organization of the tropical atmosphere. The present study investigates that possibility by using a two-dimensional, nonrotating model that includes a set of physical parameterizations carefully evaluated against tropical data. In the absence of cloud–radiation interactions, the model spontaneously generates fast upwind (eastward) moving planetary-scale oscillations through the wind-induced surface heat exchange mechanism. In the presence of cloud–radiative effects, the model generates slower upwind (eastward) propagating modes in addition to small-scale disturbances advected downwind (westward) by the mean flow. Enhanced cloud–radiative effects further slow down upwind propagating waves and make them more prominent in the spectrum. On the other hand, the model suggests that interactions between moisture and convection favor the prominence of moist Kelvin-like waves in tropical variability at the expense of small-scale advective disturbances. These numerical results, consistent with theoretical predictions, suggest that the interaction of water vapor and cloud variations with convection and radiation plays an active role in the large-scale organization of the tropical atmosphere.

1. Introduction

Tropical variability is dominated by intraseasonal time scales. The phenomena, often referred to as intraseasonal oscillations, includes the Madden–Julian Oscillation (MJO), a planetary-scale disturbance (wavenumbers 1–3) propagating from west to east with typical speeds of 5 to 10 m s^{-1}.

Despite a large number of observational studies, [see Madden and Julian (1994) and Lin et al. (2000) for a review] a comprehensive theory of the MJO has proven elusive. Early work characterized the MJO as a wave–conditional instability of the second kind Kelvin-like mode of low wavenumber (e.g., Lindzen 1974; Chang 1977), and subsequent studies introduced more realistic interactions between convection and large-scale flow in Kelvin wave MJO models (e.g., Emanuel 1987; Neelin et al. 1987; Lau and Peng 1987; Lau et al. 1988). Evidence of the coupling between convection and large-scale dynamics was presented by Wheeler and Kiladis (1999), who used space–time spectrum analysis of tropical outgoing longwave radiation (OLR) to show that the equatorially trapped wave modes of shallow water theory describe quite well the variability of deep tropical cloudiness, albeit with equivalent depth greatly reduced from what would be expected in a dry atmosphere. They also found that although moist Kelvin waves and the MJO both appear to be convectively coupled, the MJO differs from the Kelvin wave by hav-

Corresponding author address: Dančе Zurovac-Jevtić, Guy Carpenter & Company AB, Rehnsg. 11, SE-113 57 Stockholm, Sweden.
E-mail: dance.zurovac-jevtic@guycarp.com

ing approximately constant frequency for the range of planetary wavenumbers from 1 to 7.

Analysis of 15 atmospheric general circulation models (GCM) showed that all models have difficulties simulating the MJO, especially its low phase speed and its low wavenumber structure (Slingo et al. 1996). As the treatment of clouds and cloud–radiation interactions is known to be a challenging and uncertain component in climate models, several studies, using models of different complexity, have investigated the impact that the representation of moist processes might have on the simulation of the MJO.

For example, Slingo and Madden (1991) found that removing cloud–longwave radiation interactions from the National Center for Atmospheric Research Community Climate Model reduces the amplitude but does not change the period of the MJO. Chao and Lin (1994) found that the simulation of the MJO by their model is sensitive to the choice of the cumulus parameterization scheme. Raymond (2001) proposed a model in which the cloud–radiation interactions provide a large-scale instability mechanism capable of capturing the essence of the MJO phenomenon. The key characteristic in his model is the lag between enhanced surface fluxes and enhanced precipitation, entered through his convection parameterization. Employing a cloud-resolving model, Grabowski and Moncrieff (2001) found that in the absence of cloud–radiative feedbacks the deep convection organizes into two primary scales: westward propagating waves on a scale of a few hundred kilometers and eastward propagating envelopes of convection on a scale of thousands of kilometers. Interactive radiation weakens the MJO in this model (Grabowski and Moncrieff 2002). Later experiments conducted with a nonhydrostatic global model that applies a cloud-resolving convection parameterization show that MJO-like systems could appear in the absence of radiative feedbacks, but not in the absence of moisture–convection feedback (Grabowski 2003). Using a simple, zero-dimensional atmospheric model coupled to an ocean mixed layer, Sobel and Gildor (2003) show that cloud–radiation interactions along with wind-induced surface heat exchange (WISHE) and ocean interactions lead to ocean–atmospheric variability on intraseasonal time scales.

These numerical studies, in addition to observational studies (e.g., Mehta and Smith 1997; Johnson and Ciesielski 2000; Myers and Waliser 2003; Lin and Mapes 2004) suggest that convective and radiative processes play a significant role in simulation of intraseasonal variability by influencing the vertical distribution of diabatic heating and static stability. Based on a number of recent studies (Grabowski and Moncrieff 2001, 2002; Grabowski 2003; Lee et al. 2001; Bony and Emanuel 2005), a more complex picture of how the feedbacks between moisture, radiation, and convection affect the variability of the tropical atmosphere is starting to emerge.

In this paper we will use a 2D primitive equation model to simulate the tropical atmosphere circulation over an ocean surface. Two-dimensional cloud-resolving simulations have previously been used for investigating the large-scale organization of tropical deep convection (e.g., Oouchi 1999; Grabowski and Moncrieff 2001, 2002). The 2D framework does not contain a planetary vorticity gradient and thus it filters most equatorial wave disturbances. Simulated disturbances propagate in a direction predetermined by the choice of the imposed mean wind. While clearly an unrealistic representation of the equatorial atmosphere, this setup is faster and easier to use than a full GCM and it allows us to analyze how the physics of low wavenumber–low frequency variability interacts with convection, radiation, and surface fluxes in an idealized controllable framework. The model uses the Emanuel convection scheme, and Bony and Emanuel parameterization of cloudiness coupled to the convection, which test well in a single-column model driven by Tropical Ocean Global Atmosphere Coupled Ocean–Atmosphere Response Experiment (TOGA COARE) Intensive Flux Array (IFA) data (Bony and Emanuel 2001). In this study we will focus on the role moist–radiative and moisture–convection feedbacks have in the organization of the tropical disturbances. This, and not the simulation of equatorial wave disturbances, is our main objective. Also, in the spirit of maximum simplicity, we keep the sea surface temperature and the equatorial insolation constant in space and time (no diurnal or seasonal cycle); no time-varying external forcing is applied to the system. Section 2 describes the model used in this study. The influence of WISHE is discussed in section 3. Section 4 describes the effect of cloud–radiation interactions on the variability. Section 5 focuses on the role of clouds, especially the sensitivity of low frequency variability to increased upper tropospheric cloudiness. The sensitivity to moisture–convection feedbacks is tested in section 6, and a summary is given in the final section.

2. Model description and experimental setup

The 2D model used in this study is reduced from the atmospheric version of the Massachusetts Institute of Technology GCM, which is based on a novel approach in which atmosphere–ocean fluid isomorphism is used to derive, from a single hydrodynamical core, atmospheric, and oceanic counterparts (Marshall et al. 2004).

A crucial aspect of this general circulation model is that its physics package is composed of parameterizations that have been rigorously tested against real data. It includes, in particular, the convection scheme developed by Emanuel (1991) that was revised and optimized in its prediction of humidity with respect to tropical observations (Emanuel and Živković-Rothman 1999). It is based on the premise that the essential physics that controls atmospheric water vapor include turbulent entrainment, cloud microphysical processes, and the production of unsaturated downdrafts by evaporating precipitation. Based on observations of cumulus clouds (e.g., Raymond and Blyth 1986; Taylor and Baker 1991), each cloud is considered to consist of an ensemble of updrafts and downdrafts. The mixing is idealized as being episodic, so that air in each updraft and downdraft travels a finite vertical distance and then mixes with the unperturbed environment, forming a spectrum of mixtures, which then ascend or descend to their new levels of neutral buoyancy. At each step, cloud water in excess of a temperature-dependent threshold is converted to precipitation, which falls and partially or totally reevaporates according to a rate equation. This evaporation drives an unsaturated downdraft that transports enthalpy and water. The upward mass flux through the cloud base is controlled by the buoyancy of air lifted from the parcel origin level (which may vary) to a short distance above its level of free convection, thus effectively driving the system toward boundary layer quasi-equilibrium.

The model includes a statistical cloud scheme whose novelty lies in its explicit coupling to the convection scheme described above (Bony and Emanuel 2001): it represents subgrid-scale fluctuations of total water (vapor plus condensed phase) concentration by a probability density function whose mean, variance, and skewness are diagnosed (instead of assumed) from the local concentration of condensed water produced at the subgrid-scale by cumulus convection, from the degree of saturation of the environment, and from the requirement that the total water is positive (the convection scheme thus predicts the in-cloud water content produced at the subgrid scale, while the statistical cloud scheme predicts how condensed water is spatially distributed within the domain). The performance of the scheme was tested in a column model forced by TOGA COARE IFA data, showing agreement between calculated and satellite-measured radiative fluxes at the top of the atmosphere as well as reproducing some main characteristics of the cloudiness observed over the warm pool (Bony and Emanuel 2001).

Radiative cooling is computed interactively using the shortwave parameterization of Fouquart and Bonnel (1980) and the longwave parameterization of Morcrette (1991). Radiative fluxes are computed at each vertical level every two hours using instantaneous profiles of temperature, humidity, cloud fraction and cloud water path, and a climatological distribution of ozone. Maximum overlap is assumed for vertically adjacent cloud layers, while random overlap is used for nonadjacent cloud layers. The effective size of cloud particles and the temperature thresholds from which the phase of cloud water is diagnosed are specified as in Bony and Emanuel (2001).

All 2D idealized experiments are performed on an ocean-covered domain. The horizontal resolution is set to 240 grid points (with 1.5° spacing), while 40 levels equally spaced in pressure (25 hPa) are used in the vertical. The choice of this resolution was motivated by the studies of Emanuel and Živković-Rothman (1999) and Tompkins and Emanuel (2000) showing that such a resolution is necessary for accurate prediction of atmospheric water vapor. The dynamical and the physical time steps are set to 300s, except for the radiation calculations, which are executed every two hours. The upper boundary is a rigid lid at 25 hPa and a set of experiments with the sponge layer at the upper boundary showed no significant impact on the results. In the horizontal cyclic boundary conditions are used.

A basic state is created first by turning off all advection and running each atmospheric column to a state of radiative-convective equilibrium, imposing an SST of 300K. The surface drag is set to zero, and the equatorial insolation is kept constant in space and time. A vertically uniform, steady, easterly mean wind of 5 m s^{-1} is then imposed and very small random perturbations (white noise) are introduced in the initial field of potential temperature at 1000 hPa. If the mean state is unstable, these random perturbations will develop and a new equilibrium or statistical equilibrium will emerge.

All simulations were run for about 450 days. After the integrations have reached statistical equilibrium (which happens after about 180 days), samples of six months of data are extracted and analyzed. The time–longitude and spectral density plots in this paper are based on anomalies that are calculated using the simulated model data recorded every 6 h. At each grid point, the data have been detrended in time. The spectral density plots are retrieved using a wavenumber-frequency spectrum analysis method (Hayashi 1982). This is a two-step procedure requiring complex FFTs to first be performed in longitude to obtain Fourier coefficients (in horizontal planetary wavenumber space) for each time, followed by a second step in which the complex FFTs are applied in time to these coefficients to obtain the wavenumber-frequency spectrum. Finally,

TABLE 1. Summary of experiments.

Expt name	Comments
CRF_OFF	Cloud–radiative forcing is substituted by the clear-sky radiative cooling
CRF_ON	Cloud–radiation interactions are turned on
CRF_FIX	The clear-sky radiative cooling is computed interactively but the cloud radiative forcing is specified as a constant profile
CRF_OFF_noW	Same as CRF_OFF but the WISHE effect is turned off by imposing a constant horizontal wind in the computation of surface fluxes
CRF_ON_EP	Same as CRF_ON, but the maximum precipitation efficiency is reduced from 0.999 to 0.99
CRF_OFF_SIGS	Same as CRF_OFF but the moisture–convection feedback is enhanced by increasing the fraction of precipitation that falls outside the cloud and is exposed to evaporation (the parameter σ_s of the Emanuel convection scheme is increased from 0.12 to 0.30)
CRF_ON_SIGS	Same as CRF_ON but the moisture–convection feedback is enhanced
CRF_ON_EP_SIGS	Same as CRF_ON but the maximum precipitation efficiency is reduced from 0.999 to 0.99 and the moisture–convection feedback is enhanced

no red background was subtracted [as was done in the analysis of Wheeler and Kiladis (1999)] and wavenumber 0 has been removed from the plots.

3. Effects of WISHE on the model-simulated variability

Emanuel (1987) and Neelin et al. (1987) proposed the WISHE mechanism for maintaining the MJO. In classical WISHE theory, the eastward propagation of the convective regimes is assumed to be driven by wind-induced anomalies in evaporation, superimposed on mean easterlies, such that evaporation is enhanced east of the enhanced convection and suppressed west of the enhanced convection. The evaporative entropy source is partially in phase with the wave temperature, thus converting potential to kinetic energy. In this theory, the main effect of moist convection is to reduce the effective stratification felt by the waves, substantially reducing their frequency. This theory has been tested in a number of GCM and other model studies (e.g., Numaguti and Hayashi 1991; Seager and Zebiak 1994; Hayashi and Golder 1997) and the results suggest either that WISHE tends to maintain the 30–60-day oscillation or that it at least makes the low-frequency, low-wavenumber signal stronger.

To identify the role of WISHE in the wave organization simulated with our model, we compare the variability simulated by the model with and without the WISHE mechanism, in the absence of cloud–radiation interactions (these experiments are referred to as CRF_OFF and CRF_OFF_noW; see Table 1 for a summary of all numerical experiments performed with this model). In the bulk-aerodynamic formula the surface wind speed depends on both the explicitly calculated mean zonal wind and gustiness factor owing to convective downdrafts. The WISHE mechanism is turned off by specifying a constant surface wind speed (fixed to the mean background wind velocity) in the calculation of surface latent and sensible heat fluxes. In the time tendency of temperature, cloud–radiation interactions are turned off by ignoring the interaction of clouds and radiation that is calculated by the model (the net radiative cooling is replaced by its clear-sky value).

The steady state of experiment CRF_OFF_noW exhibits some stochastic variability in the horizontal wind field, but no propagating waves organized at the planetary scale. The dominant variability consists rather in small-scale disturbances (high wavenumbers and high frequencies) traveling westward.

In the presence of WISHE, on the other hand (but still in the absence of cloud–radiation interactions, experiment CRF_OFF), the mean initial state evolves spontaneously into a new state, characterized by a predominance of eastward propagating disturbances of planetary scale.[1] Figure 1a shows the Hovmöller diagram of the simulated horizontal wind anomalies at the 1000-hPa level. The spectral analysis in Fig. 2a confirms that the largest spectral amplitude is found at wavenumber 1, with some additional power at wavenumbers 2 and 3. An eastward-propagating phase speed of about 35 m s^{-1} (relative to the mean flow) is identified from this plot, corresponding to a period of 13–14 days. The absence of slower moist gravity waves may mean that the convective heating is only playing a small role in the wave dynamics, or that the WISHE effect is increasing the phase speed of moist modes (Emanuel 1987). The

[1] In this nonrotating framework, the only difference between east and west is our choice of an easterly background flow, which affects the disturbances through the WISHE mechanism. Although, technically, we should distinguish the propagation directions by upwind and downwind, we use the more conventional terms east and west here.

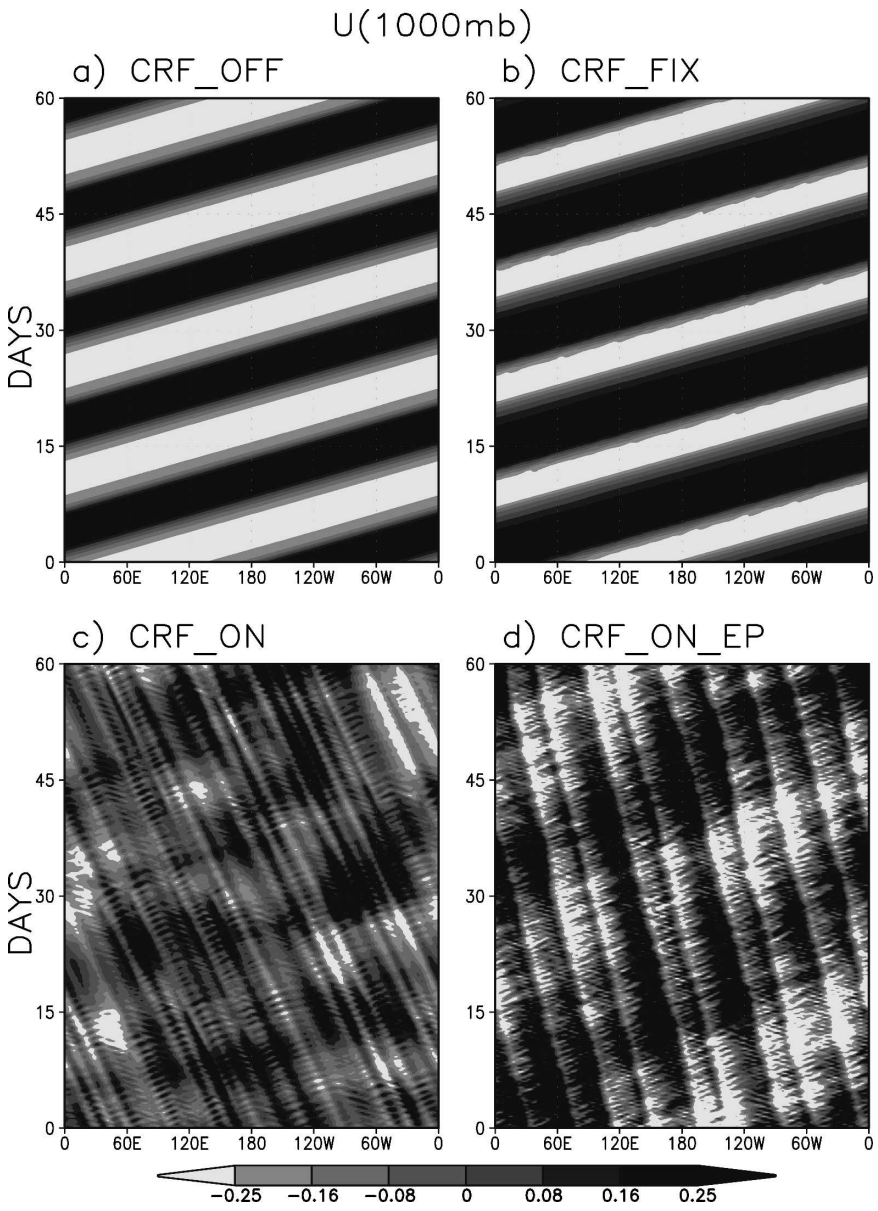

FIG. 1. Longitudinal–time diagrams of the horizontal wind perturbation (m s^{-1}) at 1000 hPa obtained from experiments (a) CRF_OFF, (b) CRF_FIX, (c) CRF_ON, and (d) CRF_ON_EP. The wind perturbations oscillate with amplitude of about 0.5 m s^{-1} in all four experiments.

vertical structure of the horizontal wind perturbations (Fig. 3, left panel) exhibits a baroclinic structure with anomalies of opposite sign in the lower and upper troposphere. The wave is tilted eastward with height, and the horizontal velocity perturbations change sign at about 500 hPa.

These experiments show that in the absence of cloud–radiation interactions, the WISHE mechanism is sufficient to organize the atmosphere into fast propagating oscillations of planetary scale. These waves are reminiscent of tropical Kelvin waves predicted by the equatorial shallow-water theory. Such waves, moving eastward at about 40 m s^{-1}, have been found in observations of the upper tropospheric temperature (Bantzer and Wallace 1996) and in station wind and pressure data over the eastern Pacific (Milliff and Madden 1996). Wheeler and Kiladis (1999) show that this mode dominates the spectra of equatorial dynamical fields, and they interpret it as the peak projection response to deep convective heating. They suggest that the wave-

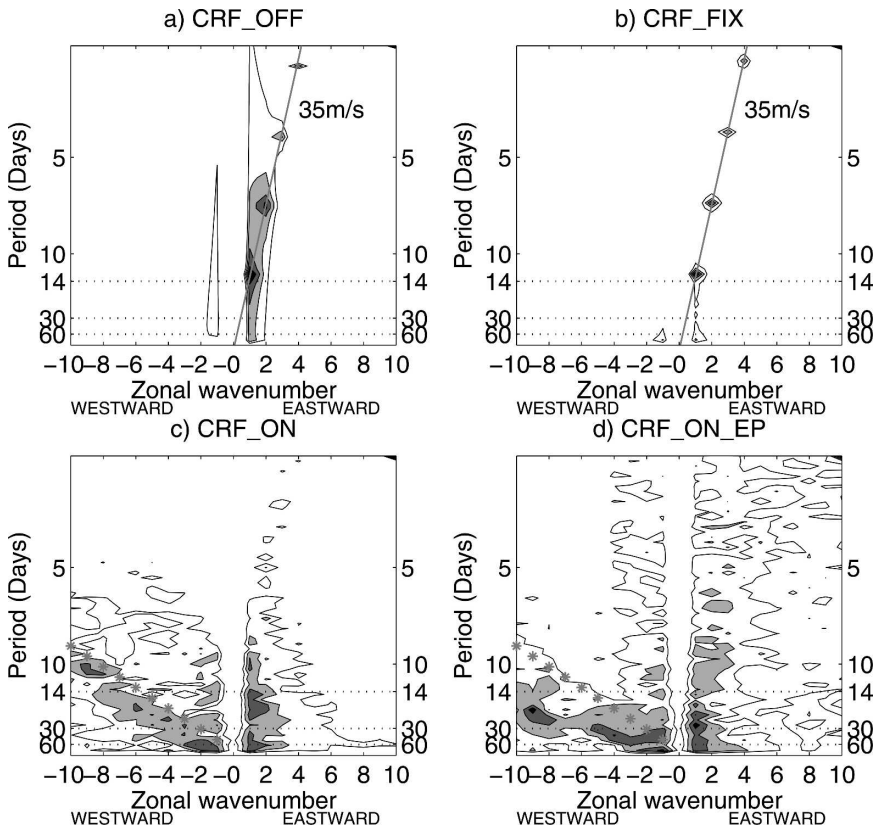

FIG. 2. Spectral analysis of horizontal wind perturbations at 1000 hPa [as natural logarithm of the spectral powers (units: $m^2 s^{-2}$)] obtained from experiments (a) CRF_OFF, (b) CRF_FIX, (c) CRF_ON, and (d) CRF_ON_EP. The asterisks on the left-hand side of (c) and (d) represent the phase speeds corresponding to the imposed mean easterly flow of 5 $m s^{-1}$. (Contours are drawn in the range of −7 to −4; shadings start at −6.)

number-frequency characteristics of this mode are distinct from those of convectively coupled equatorial waves identified in the OLR.

4. Influence of cloud–radiation interactions

Cloud–radiation interactions are known to modulate the tropospheric radiative cooling (e.g., Gray and Jacobson 1977). They produce a radiative heating within and below the cloud layer and a radiative cooling at the cloud top. Johnson and Ciesielski (2000) show that in deep convective atmospheres, the radiative heating of clouds substantially weakens the net tropospheric radiative cooling.

In the next pair of experiments, we analyze how cloud–radiation interactions influence the variability simulated by the model. In the presence of cloud–radiation interactions (experiment CRF_ON, lower left panel of Fig. 1), small-scale disturbances propagating westward dominate the variability, and eastward propagating waves are much less prominent than in experiment CRF_OFF. The power spectrum indicates that the peak power of wavenumber-1 disturbances is greatly reduced and shifted from a well-defined period of 13–14 days to a broadband period in the 10–80-day range. A similar shift in the spectral power toward lower frequencies is observed for wavenumber 2 as well. Interactions between clouds and radiation thus make the fast WISHE waves much less prominent than before, and dramatically shift the frequency of planetary-scale eastward propagating waves toward lower frequencies (Fig. 2c). The wavenumber-frequency spectral analysis reveals that in this experiment the small-scale disturbances are advected by the background flow, with a weak (about 1 $m s^{-1}$) eastward velocity relative to the mean flow (Fig. 2c). The asterisks on the left side of Fig. 2c represent the phase speeds corresponding to the imposed mean easterly flow of 5 $m s^{-1}$. The predominance of small-scale advective modes is even more apparent in the variability of upper-tropospheric wind and nondynamical fields such as precipitation or radiation.

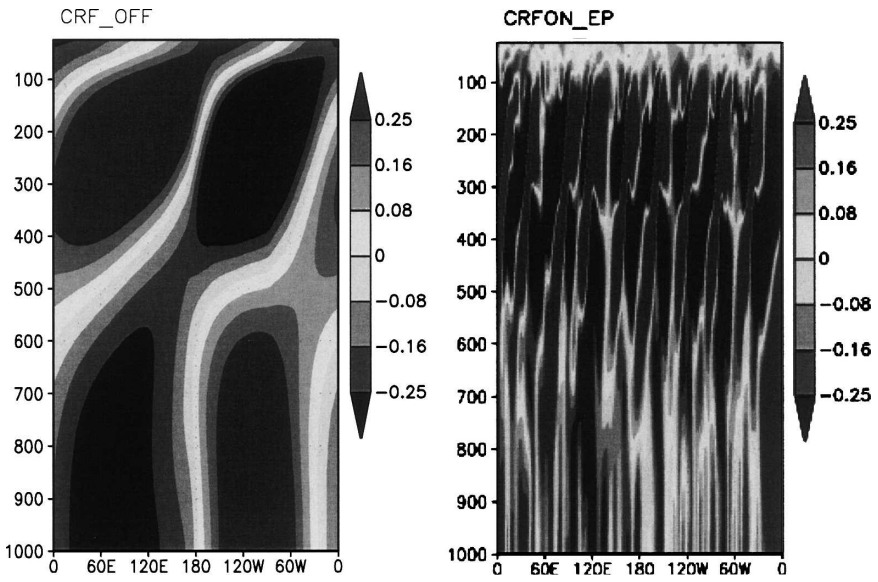

FIG. 3. The vertical structure of the horizontal wind perturbations (m s^{-1}) in the experiments (left) CRF_OFF and (right) CRF_ON_EP.

Recent studies using a large range of models of different complexity have presented consistent results. Using a linear model, Bony and Emanuel (2005) found that the primary effect of moist-radiative feedbacks was to reduce the phase speed of large-scale tropical disturbances and to excite small-scale disturbances advected with the mean flow. Lee et al. (2001) found that feedbacks between clouds and the longwave radiative forcing produced small-scale disturbances advected westward by the easterly flow, and a slowing of the wavenumber-1 disturbance propagating eastward in an aquaplanet GCM.

Using a cloud-resolving model, Grabowski and Moncrieff (2001, 2002) found that a state in which westward-propagating waves on a scale of a few hundred kilometers and eastward-propagating envelopes of convection on a scale of thousands of kilometers appear only when prescribed radiation is used. Fuchs and Raymond (2002) used a simple 2D nonrotating model of a moist equatorial atmosphere and found that when cloud–radiation effects and WISHE are turned on, the phase speeds of the modes generated by the WISHE mechanism do not decrease. But they find, as we do, that the modes with small wavelengths are stationary.

We now test whether the effect of cloud–radiation interactions is caused by its influence on the mean atmospheric state, or radiative feedbacks with convection and dynamics. For this purpose, we perform a simulation, CRF_FIX, in which the clear-sky radiative cooling is simulated interactively, but in which the cloud–radiative forcing is specified using a constant profile (which corresponds to the time-mean vertical profile of the net cloud–radiative forcing, defined as the difference between the actual radiative heating in CRF_ON and that used in experiment CRF_OFF).

Table 2 shows some of the mean characteristics of the model atmosphere in all three experiments over a three-month period. In the experiment with no cloud–radiation interactions, the mean cooling rate of the troposphere is substantially enhanced, and the magnitude of surface heat fluxes is increased accordingly. In addition, the mean precipitation rate is larger and the mean

TABLE 2. Mean characteristics of the atmosphere in the experiments CRF_OFF, CRF_FIX, and CRF_ON with relative humidity (RH) and temperature T given for each model level (700, 500, and 200 hPa).

Expt	Latent heat flux (W m^{-2})	Precipitable water (kg m^{-2})	Cloud-base mass flux (g m^{-2} s^{-1})	RH (%)			T (K)		
				700 hPa	500 hPa	200 hPa	700 hPa	500 hPa	200 hPa
CRF_OFF	121	39.4	10.9	56.2	24.7	71.6	280.9	266.5	218.5
CRF_FIX	107	46.0	9.75	67.1	43.4	73.6	281.7	266.4	219.1
CRF_ON	104	46.6	9.76	65.0	54.8	72.6	282.0	267.0	219.8

precipitable water in the troposphere is significantly smaller in experiment CRF_OFF. On average, the lower troposphere is about one degree warmer and about 10% moister in experiments CRF_FIX and CRF_ON than in CRF_OFF. An even larger difference is noted in the mean relative humidity around the 500-hPa level: in CRF_OFF, the midtropospheric relative humidity is very low, about 25%, while it is around 43% for fixed clouds and is more than doubled (about 54%) for the case of time varying clouds. Both experiments with CRF included are somewhat warmer in the upper troposphere.

This comparison confirms that although the mean states in CRF_ON and CRF_FIX are quite similar, they exhibit very different variability, as shown by both the Hovmöller diagrams (Figs. 1b,c) and the power spectra (Figs. 2b,c). The simulated variability in CRF_FIX more closely resembles that of CRF_OFF than of CRF_ON. The prominent mode of variability is a planetary-scale wave that circles the equator in 13–14 days, although the spectral analysis indicates somewhat smaller amplitude in the experiment with fixed clouds than in the experiment with no cloud–radiative forcing. This shows that the effect of cloud–radiation interactions on the mean atmospheric state only is not sufficient to explain the drastic change in wave characteristics between CRF_OFF and CRF_ON, and that it is the time-varying cloudiness that is responsible both for slowing down the eastward-propagating planetary wave and exciting smaller-scale advective modes.

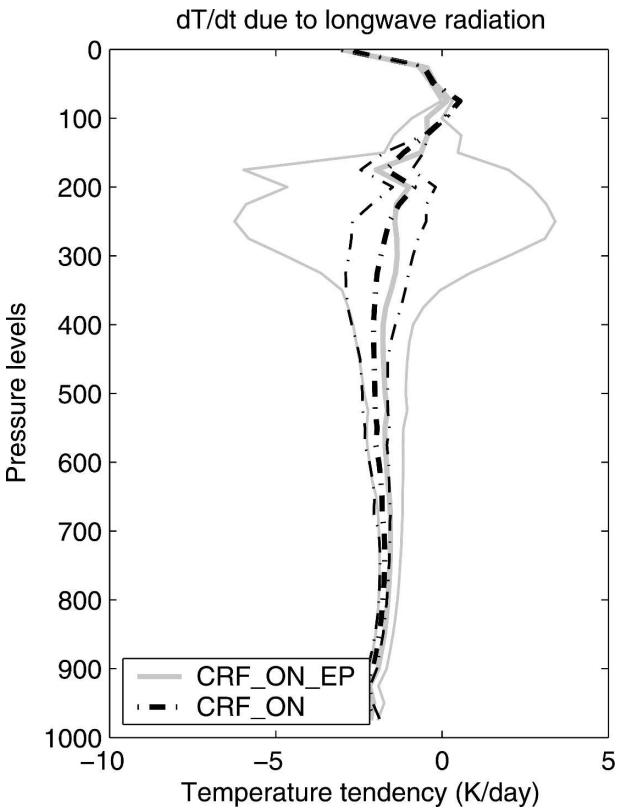

FIG. 4. Three-month mean (thick) and std dev (thin) of the temperature tendencies in the experiments CRF_ON (dashed dotted) and CRF_ON_EP (solid).

5. Sensitivity to the strength of cloud–radiation interactions

In this set of experiments we examine, in more detail, the influence of time-varying clouds on radiation, and especially the effects that thicker and more extensive upper-tropospheric cloudiness have on the simulated variability.

To increase the fractional cloudiness at upper levels, we alter the maximum value of the parcel precipitation efficiency in the Emanuel convection scheme. The fraction ε_i of condensed water that is converted to precipitation at level i, is given by

$$\varepsilon_i = \left[1 - \frac{l_c(T_i)}{\mathrm{CLW}_i}\right]\varepsilon_{\max}, \tag{1}$$

where T_i is the temperature, l_c is the temperature-dependent threshold of cloud water above which precipitation occurs (the autoconversion threshold), and CLW_i is the in-cloud condensed water mixing ratio. The maximum precipitation efficiency $\varepsilon_{\max}$ is set to a value slightly less than unity (0.999) to allow some cloud water to remain in suspension in the upper troposphere instead of being entirely rained out. This value was chosen to optimize predictions of outgoing longwave radiation in tests using TOGA COARE data (Bony and Emanuel 2001).

In experiment CRF_ON_EP, the maximum precipitation efficiency is reduced from 0.999 to 0.99. This yields more detrained condensed water, and the upper troposphere becomes moister and cloudier. Compared with the less cloudy case (CRF_ON), the mean cloud cover for a three-month period in the experiment CRF_ON_EP increases by between 5% and 25% within the 150- to 400-hPa layer. This leads to a mean column net radiative flux change from about -112 W m^{-2} in CRF_ON to about -100 W m^{-2} in CRF_ON_EP. The mean longwave radiative flux profile does not change significantly from one experiment to another (Fig. 4) and, as expected, the increased cloudiness results in about 0.5 K day^{-1} smaller cooling. The temperature shows much larger variability, especially in the upper troposphere, being about 5 times larger at around 250 hPa in CRF_ON_EP than in CRF_ON.

The Hovmöller diagram in Fig. 1d shows that the

radiative effect of more extensive upper-tropospheric cloudiness leads to a larger selectivity of certain wavenumbers. The dominance of both eastward propagating wavenumber 1 and westward-propagating wavenumber 9 is established (Fig. 2d). The spectral peak of eastward wavenumber 1 is stronger and more concentrated around a 30-day period compared with the broadband signal in the case with fewer clouds. Superimposed on the eastward moving oscillation is a westward moving wavenumber 9, which also shows larger spectral amplitude and is slower, moving eastward relative to the mean flow with a phase speed of approximately 3 $m\,s^{-1}$. Our results show therefore that the relative prominence of the different modes of variability is sensitive to the intensity of cloud–radiative feedbacks. Lee et al. (2001) noted also that the relative strength of small-scale advective disturbances compared to planetary-scale eastward propagating disturbances was highly sensitive to the intensity of cloud–radiative feedbacks in their GCM.

The horizontal wind perturbations once again exhibit a first baroclinic mode–like structure in both experiments. The new state is dominated by wavenumber 9 (as opposed to wavenumber 1 in CRF_OFF), and, as before, the waves are tilted eastward, but the horizontal wind anomaly now changes sign around 300 hPa as opposed to 400 hPa in case of fewer clouds (Fig. 3, right panel). The fields of precipitation and of horizontal wind perturbations at the 250-hPa level are dominated by the smaller-scale advective modes (not shown).

Clearly, the variability in this model is sensitive to the amount and optical properties of high-level clouds, and as the growth rate of both small-scale and planetary-scale waves increases with the intensity of cloud–radiation interactions in case of strong feedbacks the small scales are likely to hide the planetary organization of the equatorial atmosphere.

6. Sensitivity to moisture–convection feedbacks

The effect of convection on atmospheric water vapor has been studied extensively. The environmental humidity is regulated by the two competing effects: warming and drying caused by cloud-induced subsidence and moistening of the atmosphere by detrainment of water in all three of its phases. On the other hand, the moisture content in the environment regulates the rate at which convective parcels lose buoyancy through entrainment, controls the reevaporation of the falling precipitation, and affects the rate at which the convective downdrafts cool and dry the subcloud layer.

Recently, a number of studies (Tompkins 2001; Grabowski 2003; Grabowski and Moncrieff 2004; Bony and Emanuel 2005) have investigated the role of the feedbacks between deep convection and tropospheric moisture, and concluded that the sensitivity of convection to moisture might be essential for the large-scale organization of tropical convection. To address this issue, we performed a set of experiments in which the sensitivity of the convection scheme to environmental humidity and thereby moisture–convection feedbacks is enhanced. For this purpose, we follow the procedure proposed by Grabowski and Moncrieff (2004): we increase the fraction of precipitation that falls outside the cloud and is exposed to evaporation in the subsaturated downdraft. Practically, this is done by setting the parameter σ_s of the Emanuel scheme (the fraction of rain that falls through the environment) to 0.30 instead of its standard value 0.12. Although this parameter has been optimized against the TOGA COARE data (Emanuel and Živković-Rothman 1999), this simple procedure helps quantify sensitivity to moisture–convection feedbacks.

To account for the possible interaction between the enhanced moisture–convection feedbacks and the cloud–radiation interactions, we ran the following experiments with increased σ_s (in the following, the suffix SIGS refers to the increased σ_s): CRF_OFF_SIGS (cloud–radiation interactions turned off), CRF_ON_SIGS (cloud–radiation interaction at work in situations with thin upper-level clouds), and CRF_ON_EP_SIGS (cloud–radiation interaction turned on in situations with thicker clouds). The analysis of the results is summarized in Figs. 5 and 6, and should be compared with Figs. 1 and 2, which show results with standard moisture–convection feedbacks.

To illustrate the effect of the moisture–convection feedback on the mean state in the experiments with variable cloud cover, we show the mean relative humidity, temperature, cloud cover, and longwave radiative cooling profiles for a three-month period in Fig. 7. Below 200 hPa, the relative humidity fluctuations are largely determined by the moisture–convection feedback, with the experiments with smaller σ_s (CRF_ON and CRF_ON_EP) being, on average, 20% drier than the two experiments with increased σ_s (CRF_ON_SIGS and CRF_ON_EP_SIGS). The mean upper-tropospheric cloudiness (between 100 and 400 hPa) is, however, only slightly larger when the σ_s is increased.

The Hovmöller diagram of the horizontal wind (Fig. 5a) shows that although the eastward-propagating planetary-scale WISHE modes seen in Fig. 1a can still be recognized, smaller-scale oscillations propagating in both directions are clearly contaminating the pattern. Figure 6a shows that the eastward propagating waves

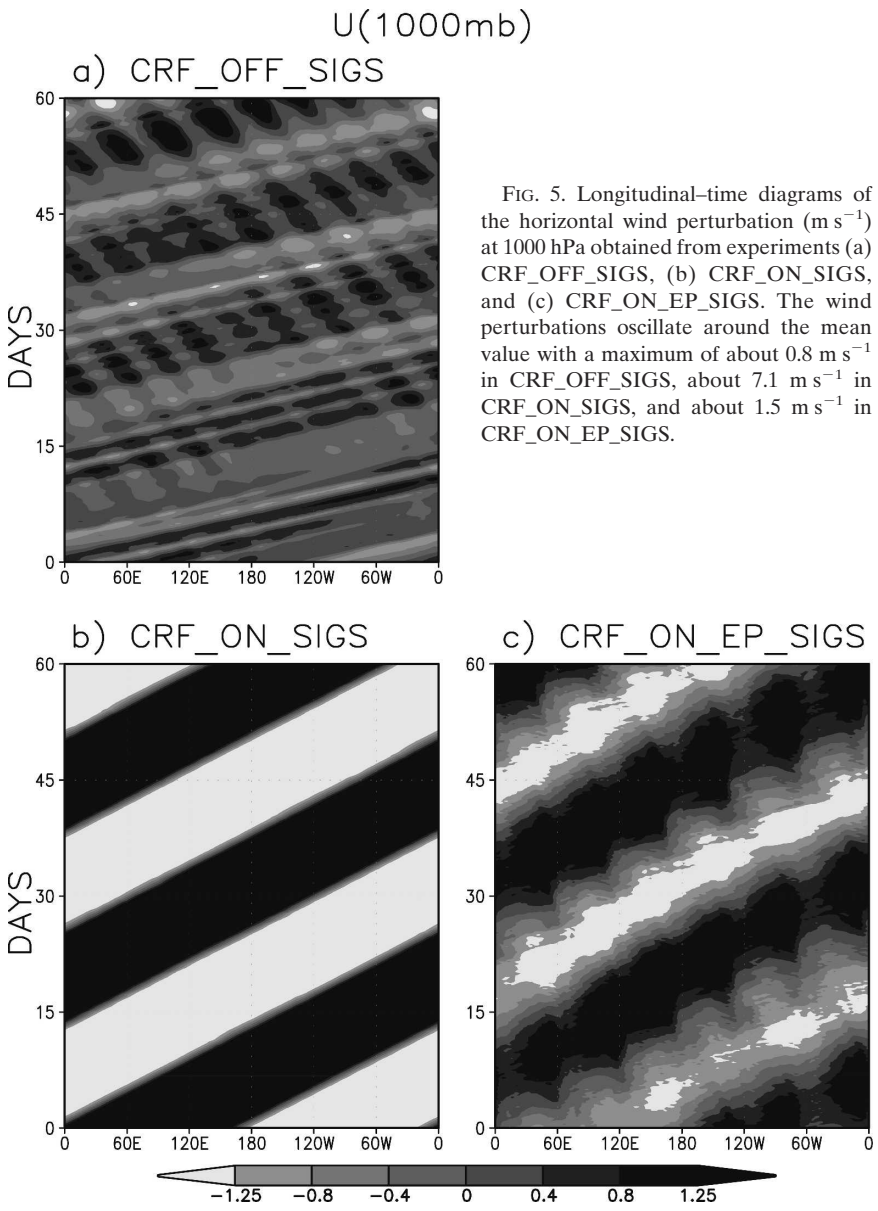

FIG. 5. Longitudinal–time diagrams of the horizontal wind perturbation ($m\ s^{-1}$) at 1000 hPa obtained from experiments (a) CRF_OFF_SIGS, (b) CRF_ON_SIGS, and (c) CRF_ON_EP_SIGS. The wind perturbations oscillate around the mean value with a maximum of about 0.8 $m\ s^{-1}$ in CRF_OFF_SIGS, about 7.1 $m\ s^{-1}$ in CRF_ON_SIGS, and about 1.5 $m\ s^{-1}$ in CRF_ON_EP_SIGS.

(1–3) feature larger spectral powers and move faster (about 45 $m\ s^{-1}$) than in the case of standard moisture–convection feedbacks (CRF_OFF). In the westward part of the spectrum, synoptic scale oscillations (wavenumbers 5–9) move at a speed somewhat higher than the imposed easterly flow of 5 $m\ s^{-1}$.

Figure 8a displays the longitudinal–time pattern of precipitation in this experiment. It shows that the prominent mode of variability in precipitation is found at wavenumber 7 and that this mode is slowly propagating westward. Thus the convection organization in this experiment is very different from that of CRF_OFF, in which the prominent mode is found at eastward-propagating wavenumber 1. Because the pattern of precipitation variability resembles the westward-moving features seen in the low-level wind pattern, it is plausible that the latter is excited because of the preference of convection to organize into small-scale westward-propagating oscillations in the presence of increased moisture–convection feedbacks. It also shows that small-scale advective modes can appear even in the absence of cloud–radiative forcing. In this case, however, the advective modes are a direct result of moisture–convection feedbacks. This is consistent with the finding of Bony and Emanuel (2005, their Fig. 8) that in the absence of moist-radiative feedbacks, interactions between moisture and convection excite modes of very slow phase speed (and thus mostly advective modes) at

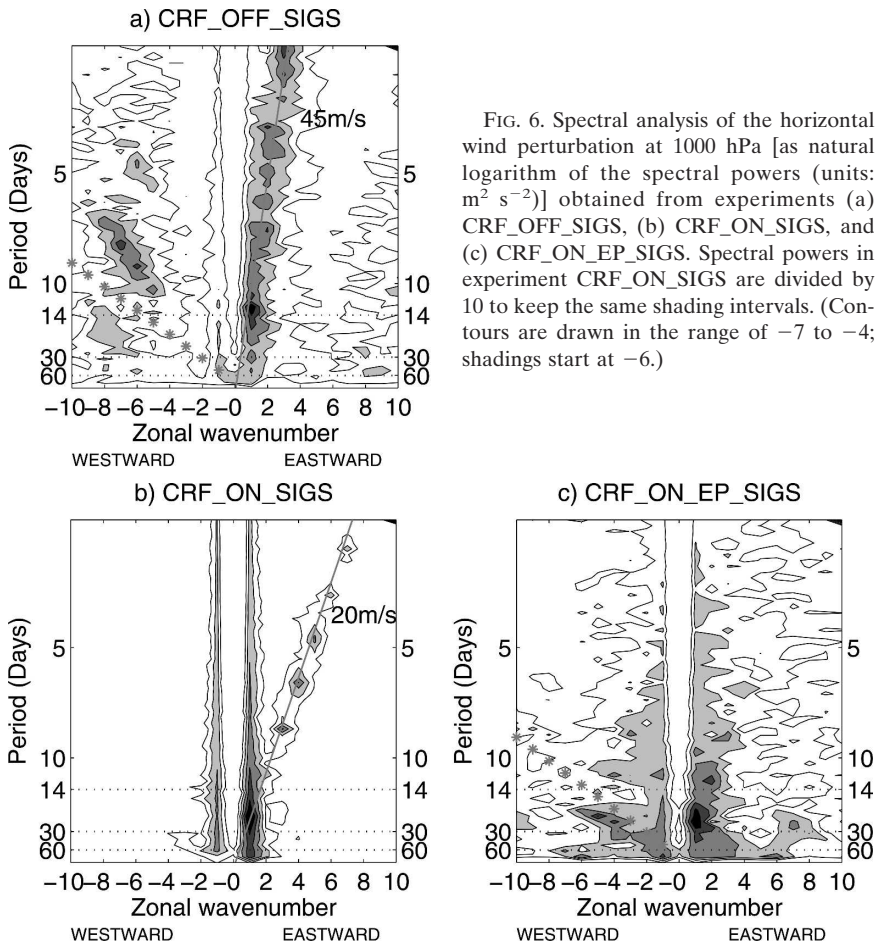

FIG. 6. Spectral analysis of the horizontal wind perturbation at 1000 hPa [as natural logarithm of the spectral powers (units: $m^2\ s^{-2}$)] obtained from experiments (a) CRF_OFF_SIGS, (b) CRF_ON_SIGS, and (c) CRF_ON_EP_SIGS. Spectral powers in experiment CRF_ON_SIGS are divided by 10 to keep the same shading intervals. (Contours are drawn in the range of −7 to −4; shadings start at −6.)

wavenumbers 3–7. A wave that was advected by the mean flow and for which the moisture–convection feedback was clearly important was also simulated by Sobel and Bretherton (2003) in a simple model setup and in the absence of cloud–radiation feedback.

Figure 5b shows the time evolution of the horizontal wind perturbations at 1000 hPa in CRF_ON_SIGS, in which both cloud–radiative and enhanced moisture–convection feedbacks are included. The equilibrium state is clearly dominated by planetary-scale oscillations propagating eastward at about 20 m s^{-1} (Fig. 6b). This wave is significantly slowed down, from a period of about 14 days in CRF_OFF_SIGS to a period of about 25 days in experiment CRF_ON_SIGS. The spectral analysis also reveals power at eastward propagating wavenumbers 2–6. All of the waves are aligned along the phase speed line of 20 m s^{-1}, characteristic of moist gravity waves. The convective organization is quite different as well, and the Hovmöller diagram in Fig. 8b shows that the precipitation pattern once again resembles the low-level wind variability but with a slight phase delay.

Thus, it appears that both cloud–radiation interactions [cf. to CRF_OFF_SIGS (Fig. 5a)] and moisture–convection feedbacks [cf. to CRF_ON (Fig. 1c)] act to decrease the phase speed and to increase the spectral amplitude of the planetary-scale wave. At the same time, moisture–convection feedbacks seem to damp the small-scale westward moving perturbations (as they are absent in the CRF_ON_SIGS) in the case when cloud–radiation interactions are not very strong. To test this further, we conducted the experiment CRF_ON_EP_SIGS, in which larger and optically thicker clouds are produced. Figures 5c and 6c demonstrate that the small-scale features clearly reappear, confirming that in the presence of the strong cloud–radiation interactions the moisture–convection feedbacks are not able to completely suppress the small-scale features. The spectral analysis in Fig. 6c also shows that, compared with Fig. 6b, the amplitude of wavenumber 1 is smaller, the higher wavenumbers are missing, and in the westward part of the spectrum advective modes of wavenumber 1–6 have appeared. Compared with CRF_ON_EP, larger and optically thicker clouds lead to increased

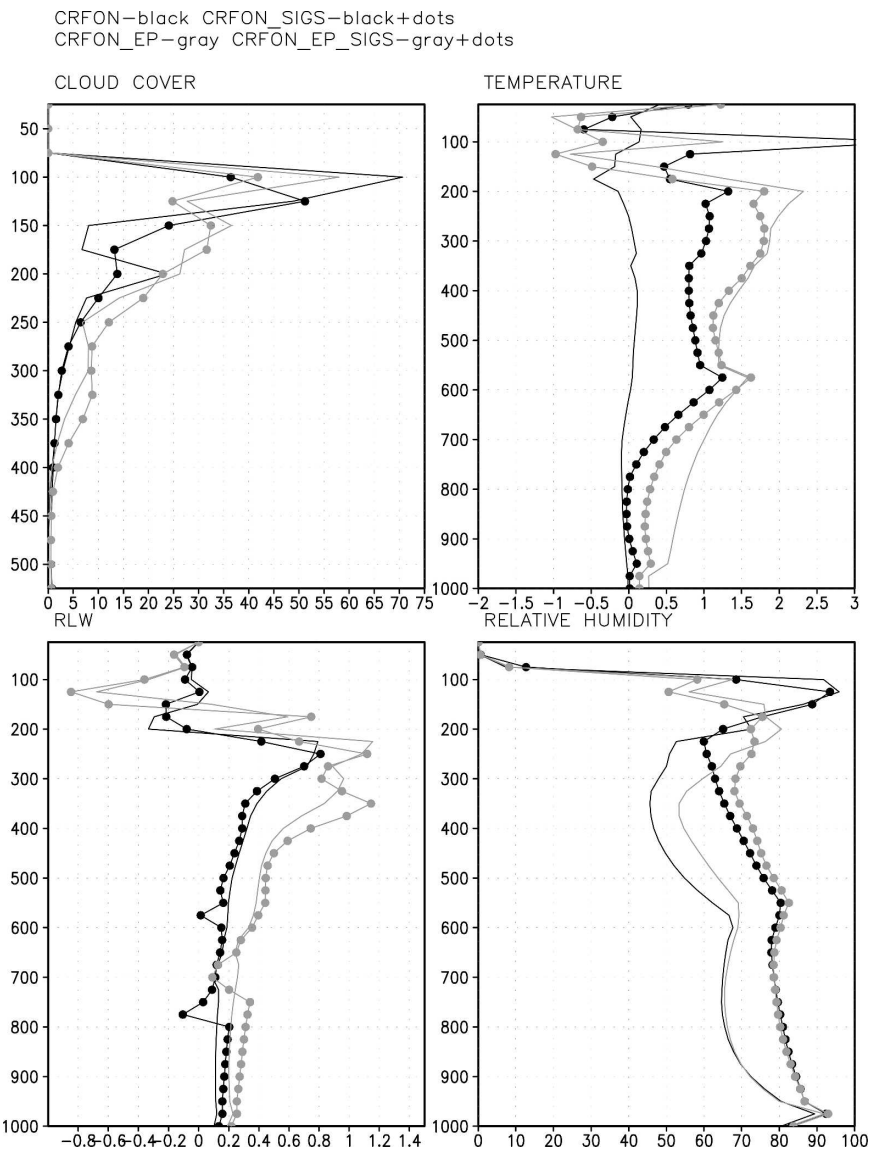

FIG. 7. Three-month mean profiles of the cloud cover, temperature deviation from the initial mean (K), warming due to net longwave radiation (K day^{-1}), and relative humidity (%) in the experiments CRF_ON (black line), CRF_ON_SIGS (black dotted line), CRF_ON_EP (gray line), and CRF_ON_EP_SIGS (gray dotted line).

selectivity of the planetary scale wave but with a somewhat shorter period (the maximum is found at a 24-day period, as compared to 27 days in CRF_ON_EP).

We conclude that in this model the relative prominence of large-scale features as compared with the small-scale features is determined by the relative strength of the cloud–radiation and moisture–convection interactions. These results are similar to those found in the linear stability analysis by Bony and Emanuel (2005). They found that the primary effect of moist–radiative feedbacks is to reduce the phase speed of large-scale tropical disturbances, by reducing the radiative cooling of the atmosphere during the rising phase of the oscillations, when the atmosphere is moister, and increasing it during periods of large-scale subsidence, when the atmosphere is drier. This reduces the effective stratification felt by propagating waves and slows down their propagation. The second effect is to excite small-scale advective disturbances traveling with the mean flow. Thus the relative preponderance of planetary waves is likely to depend on the strength of moist–radiative feedbacks.

On the other hand, the moisture–convection feedbacks seem to weaken the ability of radiative processes

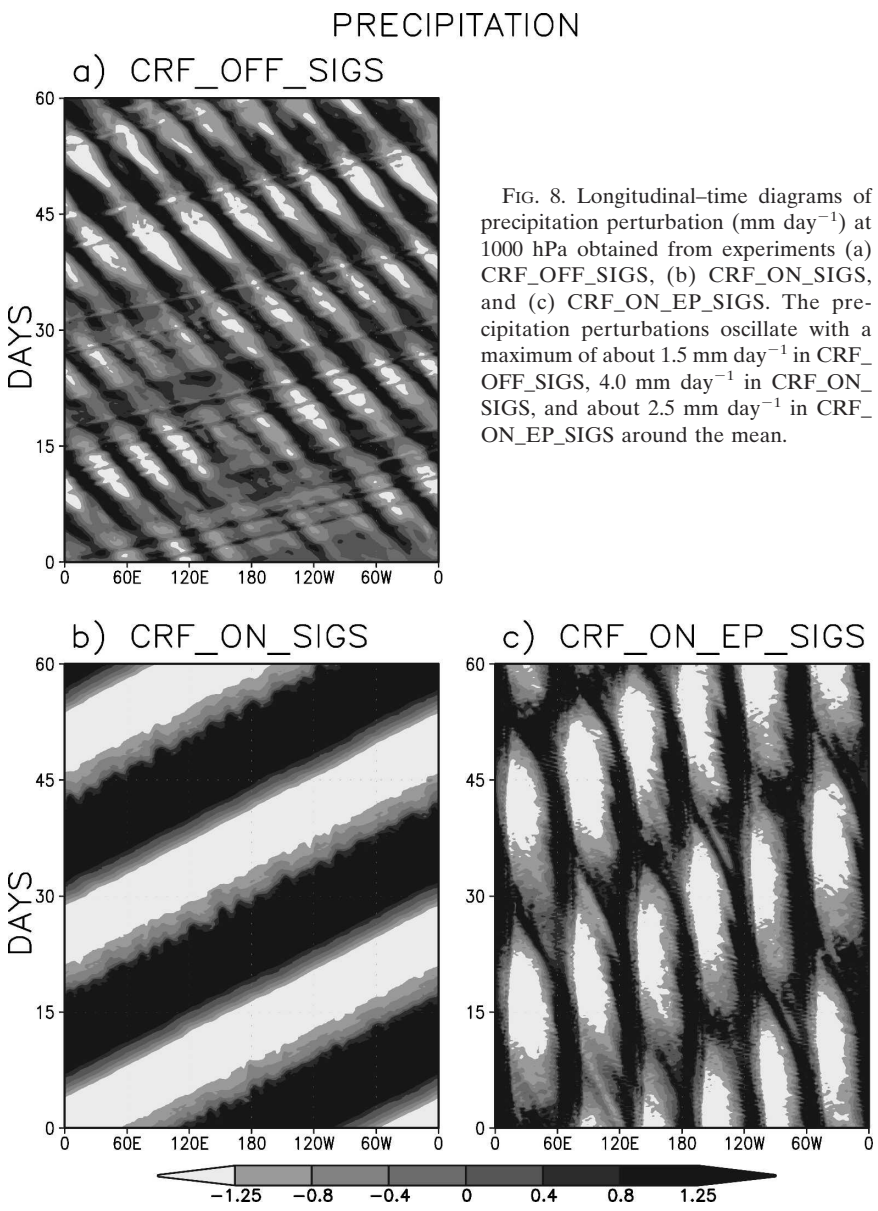

FIG. 8. Longitudinal–time diagrams of precipitation perturbation (mm day^{-1}) at 1000 hPa obtained from experiments (a) CRF_OFF_SIGS, (b) CRF_ON_SIGS, and (c) CRF_ON_EP_SIGS. The precipitation perturbations oscillate with a maximum of about 1.5 mm day^{-1} in CRF_OFF_SIGS, 4.0 mm day^{-1} in CRF_ON_SIGS, and about 2.5 mm day^{-1} in CRF_ON_EP_SIGS around the mean.

to slow down planetary-scale disturbances. To explain this feature, Bony and Emanuel (2005) considered how convection affects the moist entropy deficit of the troposphere. On average, the moist entropy has a minimum in the middle troposphere and the vertically averaged moist entropy is smaller in the free troposphere than in the subcloud layer. Therefore, convective updrafts increase the free tropospheric entropy while downdrafts decrease the subcloud layer entropy. Vertical motions tend to oppose the moist entropy deficit of the troposphere. The modulation of the precipitation efficiency by moisture fluctuations amplifies the damping term of the perturbation entropy gradient between the subcloud layer and the free atmosphere, and hence amplifies the effect. The interaction between moisture and convection thus reduces the amplitude of the moist entropy deficit anomalies and with it the magnitude of the radiative feedbacks. The above mechanisms suggest that the variability of the tropical atmosphere largely depends on the relative strength of the moisture–convection and cloud–radiation feedbacks.

In general terms, given the magnitude of equilibrium wind perturbations, the modes, which develop in this model, are too weak to explain the observed variances of intraseasonal oscillations. There are at least two possible explanations for this. One is that the weaker modes develop because the model itself is 2D, and a 3D version of the model would develop stronger modes;

the other is that the Emanuel convection scheme still underestimates the sensitivity of convection to tropospheric humidity, as suggested by Derbyshire et al. (2004). Further experiments with a 3D version of the model and stronger coupling between convection and environmental humidity in the Emanuel scheme would help understanding this problem.

7. Summary

This study focuses on the physics of low-wavenumber, low-frequency variability in a 2D aquaplanet model. We investigate the role of cloud–radiation and moisture–convection feedbacks in large-scale WISHE-generated variability.

In the absence of cloud–radiative feedbacks and when the feedbacks between moisture and convection are modest, surface horizontal wind perturbations are dominated by planetary-scale WISHE waves traveling upwind with a period of 13–14 days. The corresponding phase speed matches the slow end of the phase speeds of classical dry Kelvin waves. This may mean that the convective heating is only playing a small role in the wave dynamics, or that the WISHE effect is increasing the phase speed of moist modes (Emanuel 1987). When cloud–radiation interactions are accounted for, however, the phase speed of the eastward propagating planetary-scale waves is reduced and the spectral power is distributed in a broadband in the 10–80-day range. Superimposed on this eastward-propagating feature are new westward-moving perturbations moving approximately with the mean flow. The largest spectral powers are found for wavelengths of around 4000–5000 km. These results are consistent both with the linear model results of Bony and Emanuel (2005) and with earlier numerical results found by Lee et al. (2001) and Grabowski and Montcrieff (2001). The predominance of advective small-scale structures is especially evident in the precipitation and upper-tropospheric wind fields. Our results show that these effects are specifically caused by cloud–radiation feedbacks rather than by changes in the mean state. When cloud–radiation interactions are strengthened by promoting thicker and larger clouds, the spectral peak of eastward propagating wavenumber 1 is strengthened and the wave is further slowed down and concentrated at a period of around 30 days. The spectral amplitudes of advective modes are strengthened as well.

In an experiment in which the moisture–convection feedbacks are enhanced, planetary-scale waves become very strongly marked. The spectral amplitude of wavenumber 1 is increased by an order of magnitude compared with the previous set of experiments, and small-scale features are largely filtered out. This indicates that the moisture–convection feedbacks lead to selective damping of small-scale disturbances and favor the prominence of planetary-scale propagating waves. The planetary-scale waves observed in the surface wind field have an isolated and pronounced spectral peak matching a phase speed of 20 $m\,s^{-1}$ and may correspond to the observed moist Kelvin waves in the equatorial atmosphere. In the presence of both enhanced moisture–convection feedbacks and strong cloud–radiation feedbacks, the phase speed of the eastward-moving planetary wave is not significantly affected, but its spectral amplitude is somewhat smaller, and the westward moving (advective) features reappear, although at smaller wavenumbers.

The above results show that in this model, which uses parameterizations of clouds and convection carefully evaluated against tropical data, the cloud–radiation interactions reduce the phase speeds of large-scale disturbances on the one hand, and excite small-scale disturbances traveling with the mean flow on the other. These results are consistent with those obtained by Bony and Emanuel (2005) using a simple linear model of the tropical atmosphere. Moisture–convection feedbacks also act to reduce the phase speeds of the planetary waves, and to suppress the small-scale features when cloud–radiation interactions are not very strong. However, when optically thicker clouds are present, moisture–convection interactions weaken the ability of radiative processes to slow down the propagation of planetary-scale waves.

These results indicate that the variability of the tropical atmosphere is substantially modified by cloud–radiation and moisture–convection feedbacks. The wide range of skills of current climate models in simulating the tropical variability and intraseasonal variability in particular (Lin et al. 2006) is thus likely to stem in part from differences in the representation of these feedbacks by climate models. This emphasizes the crucial importance of evaluating in climate models the representation of clouds and cloud optical properties, and the sensitivity of the parameterized cumulus convection to tropospheric humidity variations.

Acknowledgments. We thank Adam Sobel, Dave Raymond, and an anonymous reviewer for their insightful and constructive comments, which greatly improved the original manuscript. The first author also expresses gratitude to the Knut and Alice Wallenberg Foundation Postdoctoral Fellowship Program on Sustainability and the Environment, Sweden, for research funding.

REFERENCES

Bantzer, C. H., and J. M. Wallace, 1996: Intraseasonal variability in tropical mean temperature and precipitation and their relation to the tropical 40–50-day oscillation. *J. Atmos. Sci.,* **53,** 3032–3045.

Bony, S., and K. A. Emanuel, 2001: A parameterization of the cloudiness associated with cumulus convection; Evaluation using TOGA COARE data. *J. Atmos. Sci.,* **58,** 3158–3183.

——, and ——, 2005: On the role of moist processes in tropical intraseasonal variability: Cloud–radiation and moisture–convection feedbacks. *J. Atmos. Sci.,* **62,** 2770–2789.

Chang, C.-P., 1977: Viscous internal gravity waves and low–frequency oscillations in the Tropics. *J. Atmos. Sci.,* **34,** 901–910.

Chao, W. C., and S.-J. Lin, 1994: Tropical intraseasonal oscillation, super cloud clusters, and cumulus convection schemes. *J. Atmos. Sci.,* **51,** 1282–1297.

Derbyshire, S. H., I. Beau, P. Bechtold, J.-Y. Granpeix, J.-M. Piriou, J.-L. Redelsperger, and P. M. M. Soares, 2004: Sensitivity of moist convection to environmental humidity. *Quart. J. Roy. Meteor. Soc.,* **130,** 3055–3080.

Emanuel, K. A., 1987: An air–sea interaction model of intraseasonal oscillations in the Tropics. *J. Atmos. Sci.,* **44,** 2324–2340.

——, 1991: A scheme for representing cumulus convection in large-scale models. *J. Atmos. Sci.,* **48,** 2313–2329.

——, and M. Živković-Rothman, 1999: Development and evaluation of a convection scheme for use in climate models. *J. Atmos. Sci.,* **56,** 1766–1782.

Fouquart, Y., and B. Bonnel, 1980: Computation of solar heating of the Earth's atmosphere: A new parameterization. *Beitr. Phys. Atmos.,* **53,** 35–62.

Fuchs, Ž., and D. J. Raymond, 2002: Large-scale modes of a nonrotating atmosphere with water vapor and cloud–radiation feedbacks. *J. Atmos. Sci.,* **59,** 1669–1679.

Grabowski, W. W., 2003: MJO-like coherent structures: Sensitivity simulations using the Cloud-Resolving Convection Parameterization (CRCP). *J. Atmos. Sci.,* **60,** 847–864.

——, and M. W. Moncrieff, 2001: Large-scale organization of tropical convection in two-dimensional explicit numerical solutions. *Quart. J. Roy. Meteor. Soc.,* **127,** 445–468.

——, and ——, 2002: Large-scale organization of tropical convection in two-dimensional explicit numerical solutions: Effects of interactive radiation. *Quart. J. Roy. Meteor. Soc.,* **128,** 2349–2375.

——, and ——, 2004: Moisture–convection feedback in the Tropics. *Quart. J. Roy. Meteor. Soc.,* **130,** 3081–3104.

Gray, W. M., and R. W. Jacobson Jr., 1977: Diurnal variation of deep cumulus convection. *Mon. Wea. Rev.,* **105,** 1171–1188.

Hayashi, Y., and D. G. Golder, 1997: United mechanisms for the generation of low- and high-frequency tropical waves. Part I: Control experiments with moist convective adjustment. *J. Atmos. Sci.,* **54,** 1262–1276.

——, 1982: Interpretations of space–time spectral energy equations. *J. Atmos. Sci.,* **39,** 685–687.

Johnson, R. H., and P. E. Ciesielski, 2000: Rainfall and radiative heating rates from TOGA COARE atmospheric budgets. *J. Atmos. Sci.,* **57,** 1497–1514.

Lau, K.-M., and L. Peng, 1987: Origin of low-frequency (intraseasonal) oscillations in the tropical atmosphere. Part I: Basic theory. *J. Atmos. Sci.,* **44,** 950–972.

Lau, N.-C., I. M. Held, and J. D. Neelin, 1988: The Madden–Julian Oscillation in an idealized general circulation model. *J. Atmos. Sci.,* **45,** 3810–3832.

Lee, M.-I., J.-K. Kang, J.-K. Kim, and B. E. Mapes, 2001: Influence of cloud-radiation interactions on simulating tropical intraseasonal oscillation with an atmospheric general circulation model. *J. Geophys. Res.,* **106,** 14 219–14 233.

Lin, J.-L., and B. E. Mapes, 2004: Radiation budget of the tropical intraseasonal oscillation. *J. Atmos. Sci.,* **61,** 1284–1295.

——, and Coauthors, 2006: Tropical intraseasonal variability in 14 IPCC AR4 climate models. Part I: Convective signals. *J. Climate,* **19,** 2665–2690.

Lin, J. W.-B., J. D. Neelin, and N. Zeng, 2000: Maintenance of tropical intraseasonal variability: Impact of evaporation–wind feedback and midlatitude storms. *J. Atmos. Sci.,* **57,** 2793–2823.

Lindzen, R. S., 1974: Wave–CISK in the Tropics. *J. Atmos. Sci.,* **31,** 156–179.

Madden, R. A., and P. R. Julian, 1994: Observations of the 40–50-day tropical oscillation—A review. *Mon. Wea. Rev.,* **122,** 814–837.

Marshall, J., A. Adcroft, J.-M. Campin, and C. Hill, 2004: Atmosphere–ocean modeling exploiting fluid isomorphisms. *Mon. Wea. Rev.,* **132,** 2882–2894.

Mehta, A. V., and E. A. Smith, 1997: Variability of radiative cooling during the Asian summer monsoon and its influence on intraseasonal waves. *J. Atmos. Sci.,* **54,** 941–966.

Milliff, R. F., and R. A. Madden, 1996: The existence and vertical structure of fast, eastward-moving disturbances in the equatorial troposphere. *J. Atmos. Sci.,* **53,** 586–597.

Morcrette, J.-J., 1991: Radiation and cloud radiative properties in the European Centre for Medium-Range Weather Forecasts forecasting system. *J. Geophys. Res.,* **96,** 9121–9132.

Myers, D. S., and D. E. Waliser, 2003: Three-dimensional water vapor and cloud variations associated with the Madden–Julian Oscillation during Northern Hemisphere winter. *J. Climate,* **16,** 929–950.

Neelin, J. D., I. M. Held, and K. H. Cook, 1987: Evaporation–wind feedback and low-frequency variability in the tropical atmosphere. *J. Atmos. Sci.,* **44,** 2341–2348.

Numaguti, A., and Y.-Y. Hayashi, 1991: Behaviour of cumulus activity and the structure of circulation in an "aqua planet" model. Part I: The structure of the superclusters. *J. Meteor. Soc. Japan,* **69,** 541–561.

Oouchi, K., 1999: Hierarchical organization of super cloud clusters caused by WISHE, convectively induced gravity waves and cold pool. *J. Meteor. Soc. Japan,* **77,** 907–927.

Raymond, D. J., 2001: A new model of the Madden–Julian Oscillation. *J. Atmos. Sci.,* **58,** 2807–2819.

——, and A. M. Blyth, 1986: A stochastic mixing model for nonprecipitating cumulus clouds. *J. Atmos. Sci.,* **43,** 2708–2718.

Seager, R., and S. E. Zebiak, 1994: Convective interaction with dynamics in a linear primitive equation model. *J. Atmos. Sci.,* **51,** 1307–1331.

Slingo, J. M., and R. A. Madden, 1991: Characteristics of the tropical intraseasonal oscillations in the NCAR community climate model. *Quart. J. Roy. Meteor. Soc.,* **117,** 1129–1169.

——, and Coauthors, 1996: Intraseasonal oscillations in 15 atmospheric general circulation models: Results from an AMIP diagnostic subproject. *Climate Dyn.,* **12,** 422–479.

Sobel, A. H., and C. S. Bretherton, 2003: Large-scale waves interacting with deep convection in idealized mesoscale model simulations. *Tellus,* **55,** 45–60.

——, and H. Gildor, 2003: A simple time-dependent model of SST hot spots. *J. Climate,* **16,** 3978–3992.

Taylor, G. R., and M. B. Baker, 1991: Entrainment and detrainment in cumulus clouds. *J. Atmos. Sci.,* **48,** 112–121.

Tompkins, A. M., 2001: Organization of tropical convection in low vertical wind shears: The role of water vapor. *J. Atmos. Sci.,* **58,** 529–545.

——, and K. A. Emanuel, 2000: The vertical resolution sensitivity of simulated equilibrium temperature and water vapour profiles. *Quart. J. Roy. Meteor. Soc.,* **126,** 1219–1238.

Wheeler, M., and G. N. Kiladis, 1999: Convectively coupled equatorial waves: Analysis of clouds and temperature in the wavenumber–frequency domain. *J. Atmos. Sci.,* **56,** 374–399.